Research Article | Vol. 10, No. 2 | 1 Feb 2019 | BIOMEDICAL OPTICS EXPRESS 855
Biomedical Optics EXPRESS

Tissue effects of intra-tissue refractive index shaping (IRIS): insights from two-photon autofluorescence and second harmonic generation microscopy

Dan Yu,[1,2] Edward B. Brown,[3] Krystel R. Huxlin,[1,4,5] and Wayne H. Knox[1,2,5,*]

[1]*The Institute of Optics, University of Rochester, Rochester, NY 14627, USA*
[2]*Materials Science Program, University of Rochester, Rochester, NY 14627, USA*
[3]*Department of Biomedical Engineering, University of Rochester, Rochester, NY 14627, USA*
[4]*Flaum Eye Institute, University of Rochester, Rochester, NY 14627, USA*
[5]*Center for Visual Science, University of Rochester, Rochester, NY 14627, USA*
**wknox@UR.Rochester.edu*

Abstract: Intra-tissue refractive index shaping (IRIS) is a novel, non-ablative form of vision correction by which femtosecond laser pulses are tightly focused into ocular tissues to induce localized refractive index (RI) change via nonlinear absorption. Here, we examined the effects of Blue-IRIS on corneal microstructure to gain insights into underlying mechanisms. Three-layer grating patterns were inscribed with IRIS ~180 µm below the epithelial surface of *ex vivo* rabbit globes using a 400 nm femtosecond laser. Keeping laser power constant at 82 mW in the focal volume, multiple patterns were written at different scan speeds. The largest RI change induced in this study was + 0.011 at 20 mm/s. After measuring the phase change profile of each inscribed pattern, two-photon excited autofluorescence (TPEF) and second harmonic generation (SHG) microscopy were used to quantify changes in stromal structure. While TPEF increased significantly with induced RI change, there was a noticeable suppression of SHG signal in IRIS treated regions. We posit that enhancement of TPEF was due to the formation of new fluorophores, while decreases in SHG were most likely due to degradation of collagen triple helices. All in all, the changes observed suggest that IRIS works by inducing a localized, photochemical change in collagen structure.

1. Introduction

Following the success of inducing phase changes in ophthalmic hydrogels in 2006 [1,2], we proposed a new paradigm for refractive vision correction, in which corneal refractive properties can be modified without flap cutting or tissue ablation. This technique, termed Intra-tissue Refractive Index Shaping (IRIS), relies on tightly focused, low-energy femtosecond laser pulses to locally induce phase and refractive index (RI) changes in the corneal stroma via multiphoton absorption. While dopants were needed for 800 nm IRIS to enhance two-photon absorption and attain meaningful RI changes [3], Xu *et al.* [4] demonstrated that Blue-IRIS can more readily induce larger RI changes because of the significant, native two-photon absorption of cornea at 400 nm. Demonstrating feasibility of this approach, Blue-IRIS was then used to inscribe cylinder lenses in the corneas of adult cats *in vivo*; the change in refractive power of their eyes was verified with wavefront sensing and shown to persist for a year [5]. Histological analysis of Blue-IRIS in the cat cornea also showed markedly less cell death compared with femtosecond-laser in situ keratomileusis (LASIK) [6]. Meanwhile, our work in hydrogel materials demonstrated that 400 nm laser micromachining can locally decrease RI by increasing the water content of written regions, and it was assumed that this hydrophilicity was associated with depolymerization [7].

#349777 https://doi.org/10.1364/BOE.10.000855
Journal © 2019 Received 30 Oct 2018; revised 29 Dec 2018; accepted 2 Jan 2019; published 24 Jan 2019

Biomedical Optics EXPRESS

However, whether the mechanisms by which Blue-IRIS induces RI changes in cornea are analogous to those in hydrogels remains unclear. Because Blue-IRIS appears to be a promising technique for vision correction, it has become necessary to thoroughly and systematically investigate the dependence of RI change on IRIS laser scanning and other parameters, and to characterize the tissue effects underlying these RI changes.

Although thinner than human corneas (550 ± 40 μm), rabbit corneas (420 ± 20 μm) share many similarities with human corneal tissue, including microanatomy, biomechanical strength and molecular composition [8,9]. This makes the rabbit cornea a suitable model for vision correction studies. To explore the tissue effects of Blue-IRIS and its underlying mechanisms, a RI profile was built by inscribing IRIS patterns of different phase change magnitudes into the corneal stroma of *ex vivo* rabbit globes. Local structural changes were imaged and quantified using 810 nm-excited two-photon excited autofluorescence (TPEF) and second harmonic generation (SHG) microscopy. Multiphoton imaging techniques like TPEF and SHG have been shown to be sensitive probes for thick tissues and live animals due to their high axial resolution, large penetration depth and minimal photo-toxicity [10–12]. Despite the extremely low two-photon absorption probabilities, tissue and live animals normally have intrinsic fluorescent components with large effective cross-sections in the green and cyan parts of the spectrum, making TPEF feasible for in-depth and label-free tissue imaging [13]. While SHG can be used for similar spatial "optical sectioning" of thick tissues as TPEF, it can provide additional information on the amount and organization of fibrillary collagen in samples, as SHG signals originate from intrinsic, non-centrosymmetric molecular structures [14,15]. SHG sources within the focal volume generally remain phase-matched and emit coherently; however, phase-matching for backward propagation only occurs when the sources are aligned at a specific spatial frequency, thus resulting in much weaker backward-SHG (B-SHG) signals [16,17]. Although there remains some controversy in explaining the complex second harmonic response from inhomogeneous SHG sources, the magnitude ratio of forward-SHG (F-SHG) and B-SHG, mostly denoted by F/B ratio, has been used to estimate the orientation and axial size of collagen fibrils [18,19], as well as distinguishing reactive or diseased tissues from normal ones [20]. The capability of backward detection is also noteworthy, considering the difficulties of collecting F-SHG signals in many *in vivo* tissue imaging cases. Since the majority of corneal lamellae are highly-hyperpolarized type I collagen, which can emit stronger SHG signals than most SHG generators [16], TPEF and SHG together are ideal techniques to use for visualizing structural modification induced by Blue-IRIS in the corneal stroma.

2. Method

2.1 Blue-IRIS instrumentation and procedure

The femtosecond laser system used to perform IRIS (Fig. 1(a)) was comprised of a mode-locked Ti:Sapphire oscillator (Vitesse; Coherent Corporation, Santa Clara, CA, USA) emitting 800 nm, 100 fs pulses at 80 MHz. The 800 nm beam was first frequency doubled with a second harmonic generator, passing through a metallic variable neutral density filter, and finally focused into each sample with a high numerical aperture (N.A. = 1.05), water-immersion microscope objective (XLPLN25XWMP2, Olympus, Center Valley, PA, USA). With the laser beam under-filling the objective, the laser beam profile was measured using a knife-edge method [21,22] and the effective N.A. was calculated to be 0.26. Eye globes were mounted on a single-axis, nano-positioning stage on top of a two-axis, linear stage (ANT95-L-Z and ANT95XY; Aerotech Inc., Pittsburgh, PA, USA) to enable precise, large-scale motion control. During IRIS, the objective was stationary while the phase gratings were written along the x-axis with different scan speeds.

Six Dutch-belted rabbit eyeballs were obtained from an approved supplier (Technical Services Specialists, Inc. Walterboro, SC, USA). Post-mortem, the globes were immediately immersed in Optisol-GS (Bausch & Lomb Inc., Rochester, NY, USA) and shipped to our

Biomedical Optics EXPRESS

laboratory overnight on ice. All animal procedures were conducted in accordance with guidelines of the University of Rochester Committee on Animal Research, the ARVO statement for the Use of Animals in Ophthalmic and Vision Research, and the NIH Guide for the Care and Use of Laboratory Animals. Optisol-GS is a commercially available storage medium used to keep corneal tissue alive for up to 14 days [23]. Once received on-site, each globe was flat-applanated using a custom-built polycarbonate suction ring, as described in our previous publications [5,6]. The ring had a 10 mm diameter inner opening, covered by a 170 µm-thick round glass coverslip. A flat-edged needle inserted into the side of the ring provided vacuum suction to the inside of the ring. In each cornea, nine rectangular lateral grating patterns were successively inscribed into the middle of the stroma using a constant laser power of 82 ± 1 mW (corresponding to a pulse energy on the order of 1.025 nJ) and scan speeds ranging from 20 mm/s to 100 mm/s. Written from the bottom to the top, each pattern consisted of three identical layers, with the top layer written ~180 µm below the epithelial surface. With a 20 µm vertical layer separation and a 0.5 µm line spacing, uniform RI changes were obtained within each dense pattern. For corneas used for two-photon imaging, patterns were designed to be 2.5 mm long by 0.20 mm wide with 0.1 mm separation; while for phase change measurement, the patterns were larger, measuring 4 mm by 0.40 mm with 0.3 mm separation. Both experiments include a double-width pattern intentionally written as a fiducial marker.

2.2 Tissue processing

Immediately after IRIS, eye globes were first wholly submersed in Optisol-GS and preserved in the refrigerator for 90 minutes, allowing microbubbles in the IRIS zone to dissipate and the cornea to return to complete transparency. With femtosecond laser pulses, bubbles tended to be much smaller in size and exhibiting shorter lifetime compared with bubbles generated under longer pulses (*e.g.* during corneal flap cutting). This transient microbubble formation was likely due to the high degree of tensile stress confinement during femtosecond laser energy deposition, and seemed to not affect cell viability [24]. Since phase change quantification was conducted on a custom-built Mach-Zehnder Interferometer (MZI), each eyeball was bisected halfway between the cornea and optic nerve, and the anterior component containing the cornea was mounted on a custom-built wet-cell. This anterior component was fully submersed in Optisol-GS and pressure was applied to its posterior surface in order to mimic intraocular pressure, and to keep the cornea as close as possible to its natural state in the intact eye.

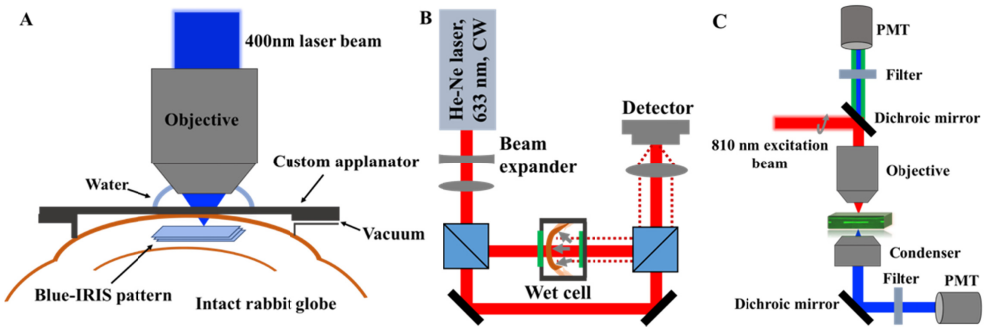

Fig. 1. (a) Blue-IRIS mounting scheme for intact rabbit globe. Globes were mounted on a three-axis translation system during raster scanning. (b) Custom-built MZI used for phase change measurement. The reference arm and test arm were recombined to form an interference pattern that contained the phase difference between two arms. (c) Two-photon microscopy system used for TPEF and SHG imaging. Immediately after each TPEF and F-SHG image stack was collected, the filter (525 nm, 100 nm bandwidth) for the backward channel was replaced with a 405 nm, 30 nm bandwidth emission filter and another SHG image stack was taken from exactly the same ROI.

Biomedical Optics EXPRESS

Globes used for microscopy were prepared by first dissecting around the scleral rim, then immersion-fixing the cornea-containing piece in 4% paraformaldehyde in Phosphate Buffered Saline (PBS, 0.1 M, pH = 7.4) for 10 minutes. The tissue was then transferred to 30% sucrose in PBS (0.1 M, pH = 7.4) at 4 °C for another 24 hours for cryo-protection before sectioning. After that, each cornea was mounted in OCT compound (Tissue Tek; Sakura Finetek, Torance, CA), frozen and sectioned into 20 µm-thick slices using a cryostat (2800 Frigocut E; Leica, Bannockburn, IL). Slide-mounted sections were then rinsed in 0.1 M PBS solution, lightly dried in an oven and cover-slipped with antifade mounting medium (VECTASHIELD H-1000, Vector Laboratories, Burlingame, CA).

2.3 Measurement of IRIS-induced phase changes

Phase change was measured on a custom-built MZI using a 633 nm He-Ne laser (Fig. 1(b)), with the mounted cornea placed on a XYZ translation stage in the test arm. An interferogram and its co-located bright field image (taken by blocking the reference arm), were collected for each IRIS pattern. Similar to the method we have used earlier to quantify phase change in hydrogels [25], the phase map corresponding to each corneal interferogram was calculated using the carrier fringe methods [26], and the induced phase change was unwrapped with the Goldstein's branch cut unwrapping algorithm [27]. To reduce the effect of low-frequency phase variations across the interferogram caused by residual aberrations and wrinkles in the cornea, each IRIS pattern was measured at 10 different positions to collect 10 pairs of phase change values with corresponding standard deviations. All these calculations were conducted automatically using a MATLAB (MathWorks, Natick, MA) program, and the same procedure was repeated on three different eyes.

2.4 TPEF and SHG microscopy

Image acquisition was performed with a Fluoview FV300 confocal scanning system interfaced with a BX61WI upright microscope (Olympus, Center Valley, PA), and the 810 nm circular-polarized beam was generated by a MaiTai Ti:Sapphire laser (Spectra Physics, Santa Clara, CA) at 100 fs, 80 MHz, passing through a Berek's compensator (Fig. 1(c)). Backscattered signal was collected by a XLUMPLFL20XW water-immersion objective (N.A. = 0.95, Olympus), while another Olympus 0.9 N.A. condenser lens was used to collect the forward scattered signal simultaneously. On the forward channel, the emission signal was separated from the excitation beam by a long-pass dichroic mirror (565 DCSX, Chroma, Rockingham, VT), passing through a 405/30 nm bandpass filter (HQ405/30 m-2P, Chroma), and was collected by a photomultiplier tube (PMT, HC125-02, Hamamatsu Corporation, Japan). Besides a short-pass dichroic mirror (670 DCSX, Chroma) used for beam separation, a 525/100 nm bandpass filter (HQ525/100 m, Chroma) was used before PMT to collect the autofluorescence signal on the backward channel. This filter was replaced with a 405/30 nm filter when collecting backward SHG. Laser power, PMT voltage, gain and offset were monitored and kept constant throughout the experiment. Using the surface scan mode, each scan took 5.36 s with a 2 µm step size, obtaining two image stacks on both channels simultaneously. Each image stack was maximum-intensity projected in ImageJ, in order to "autofocus" each stack into one comparable image. Background was defined as the average pixel counts of two equivalent laser-excited image stacks captured from an area without tissue on both channels, and maximum-intensity projected background images were subtracted from all original images to create background-subtracted TPEF, F-SHG and B-SHG images used for subsequent analysis described below. Image stacks of each IRIS pattern were collected sequentially from 4 samples of each eye, and 324 projected images were analyzed in total.

A MATLAB program was written to quantify the TPEF intensity of the IRIS patterns by manually selecting a region of interest (ROI) around IRIS patterns and extracting the histogram of each ROI (Fig. 2(a)). Since the histogram is a distribution of the number of pixels with respect to their intensity, the two peaks in the histogram correspond to the

Biomedical Optics EXPRESS

absolute TPEF intensity of IRIS grating lines and intensity of region outside the IRIS zone circled in the ROI, respectively. By fitting the histogram to a double Gaussian model using Eq. (1), coefficients (*a, b, c*) with their 95% confidence bounds can be obtained (Fig. 2(b)). Compared with simply measuring the mean intensity of one ROI that contained an IRIS pattern, this method provided more reliable quantitative data and no threshold setting was needed during the image processing. Because the natural corneal stroma fluoresced only weakly (also shown in Fig. 5) and its fluorescence intensity varied in different sections, we used the difference of means (MD) defined in Eq. (2) to express the IRIS-induced autofluorescence intensity change.

$$f(x,y) = a1\cdot\exp\left(-\left(\frac{x-b1}{c1}\right)^2\right) + a2\cdot\exp\left(-\left(\frac{x-b2}{c2}\right)^2\right) \quad (1)$$

$$MD\ (\%) = \frac{b2-b1}{b1}\times 100\% \quad (2)$$

To determine the average F-SHG and B-SHG intensity of the IRIS patterns, TPEF images were first thresholded by a blinded user, setting pixels within the IRIS patterns to 1 and pixels outside IRIS patterns to 0, to create a "fluorescence mask". Next, each SHG image was multiplied by the fluorescence mask in ImageJ to create a "masked SHG image" in which pixels that are within the IRIS pattern retain their original intensity value and are otherwise set to zero. A small ROI was then drawn around each IRIS pattern and the average pixel value of all nonzero pixels within the ROI was calculated, producing the average F-SHG intensity of the IRIS pattern. To evaluate the change in average F-SHG intensity due to the IRIS process, the average F-SHG intensity from regions outside the IRIS zones were measured by selecting two similar ROIs on either side of the IRIS region, *i.e.* at the same corneal depth along the optical axis of the eye. The average F-SHG of all pixels within the adjacent ROIs was calculated and averaged together to produce the average F-SHG intensity in non-IRIS regions. The "difference in F-SHG" (*i.e.* due to IRIS) was then the average F-SHG intensity of the IRIS pattern, minus the average F-SHG intensity in non-IRIS regions, divided by the average F-SHG intensity in non-IRIS regions, expressed as a percentage. The difference in B-SHG due to IRIS was determined in an analogous fashion from the B-SHG images.

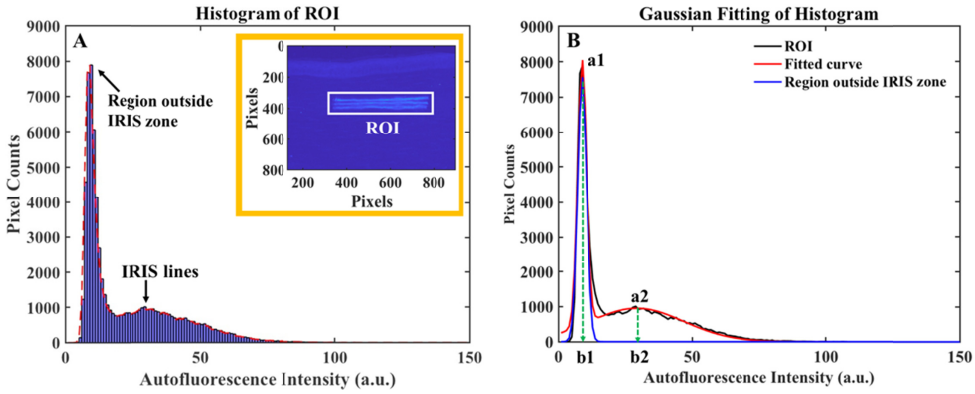

Fig. 2. (a) Histogram of one IRIS pattern written at 40 mm/s, its TPEF image is shown at the top right corner. (b) Curve fitting of the histogram.

2.5 Statistical analysis

Statistical significance of the phase change, TPEF and SHG data, as well as their interactions, were evaluated using a two-way ANOVA (JMP software, SAS, Cary, NC). Results were considered significant if $p < 0.05$.

Biomedical Optics EXPRESS

3. Results

3.1 IRIS-induced phase change as a function of scan speed

Blue-IRIS generated clear, rectangular patterns that when analyzed with the interferometer, differed from the background cornea in how they distorted the wavefront (Fig. 3). The small black spots on the interferogram were bubbles floating in the surrounding Optisol in the wet cell. Because the fringes inside the IRIS regions shifted towards the direction of decreasing optical path length, we concluded that IRIS induced a positive RI change in the rabbit cornea.

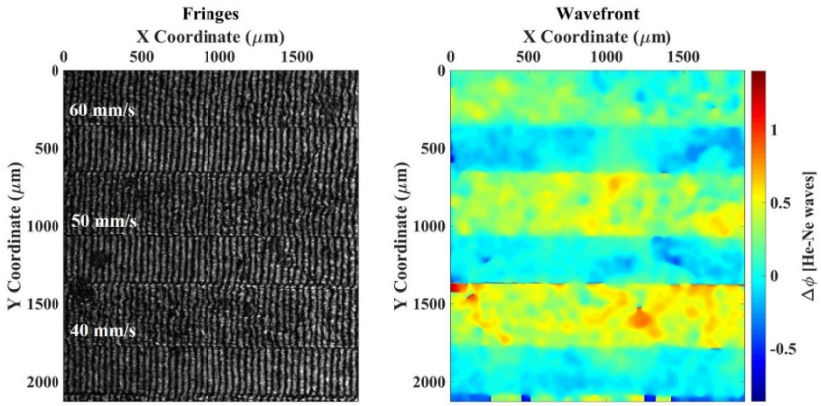

Fig. 3. Interferogram and retrieved phase map of eye 3 taken from the MZI, with scan speeds of each pattern given on the interferogram.

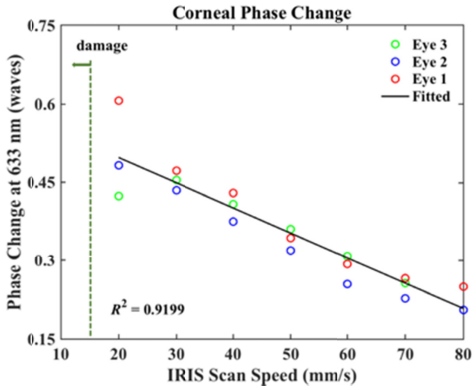

Fig. 4. Phase change measured at 633 nm as a function of scan speed, repeated on three eyes (red, blue and green data points), with a linear fit and R^2 values included in the graph. The green "damage" line indicates that at speeds below 20 mm/s, which include 10 mm/s, damage is obtained, rather than a measurable phase change.

When writing at 90 mm/s and 100 mm/s, Blue-IRIS patterns could be easily recognized on the MZI, but the phase change was so low that signal from the patterns was below the noise floor of the MZI. In contrast, damage was observed under a differential interference contrast microscope when writing at 10 mm/s. Therefore, only patterns written from 20 mm/s to 80 mm/s were quantified on the MZI in three rabbit eyes (Fig. 4). The 80 mm/s pattern in eye 3 could not be quantified due to wrinkles at the edge of the cornea; it was removed from the analysis. Despite the biological differences between individual eyes, phase change decreased sharply and significantly with increasing scan speed, with ~0.51 waves maximum phase change achieved at 82 mW and 20 mm/s. Statistically, scan speed and eye number were both significant main effects ($p_{\text{scan speed}} < 0.0001$, $p_{\text{eye number}} = 0.018$), however, their interaction was not significant. The scan speed contributed most to the induced phase change ($F_{\text{scan speed}} =$

Biomedical Optics EXPRESS

185.09, $F_{\text{eye number}} = 5.42$). Calculated by $\Delta\phi = \frac{(\Delta n)d}{\lambda}$, in which Δn is the index difference, d is the axial length of index change region parallel to optical axis and λ is the radiation wavelength [7], this corresponded to a + 0.011 RI change. Linear least-squares was used to fit each data set, and the final consolidated results indicated that Blue-IRIS-induced phase change decreased linearly with scan speed.

3.2 TPEF and SHG imaging of corneal structure

Compared with the natural corneal stroma, the three distinct Blue-IRIS layers could be readily identified by their extremely strong green autofluorescence (Fig. 5, top row). While F-SHG images exhibit striated spatial features of collagen fibers, B-SHG images result from a shorter coherence length and are more homogenous at the micrometer level. It was clear from B-SHG images that collagen lamellae were highly interwoven and exhibited certain oblique angles with respect to the corneal surface in the anterior stroma, showing a transverse ("anterior-posterior direction") lamellar arrangement, as described previously [28]. However, deeper in the stroma, lamellae were less interwoven and were organized parallel to the corneal surface.

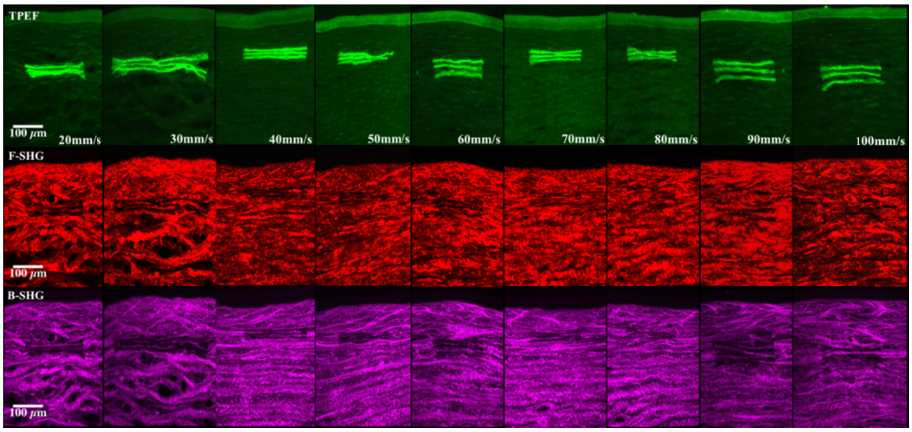

Fig. 5. TPEF (green), F-SHG (red) and B-SHG (magenta) images of the same ROIs over different IRIS patterns written at different speeds from eye 1. Note the faint green autofluorescence of the corneal epithelium on the top of all TPEF images, which contrasts with the strong TPEF signal emanating from the IRIS patterns. Note also the decreased SHG signal coincident with each IRIS pattern. Scale bar: 100 μm for all images.

Biomedical Optics EXPRESS

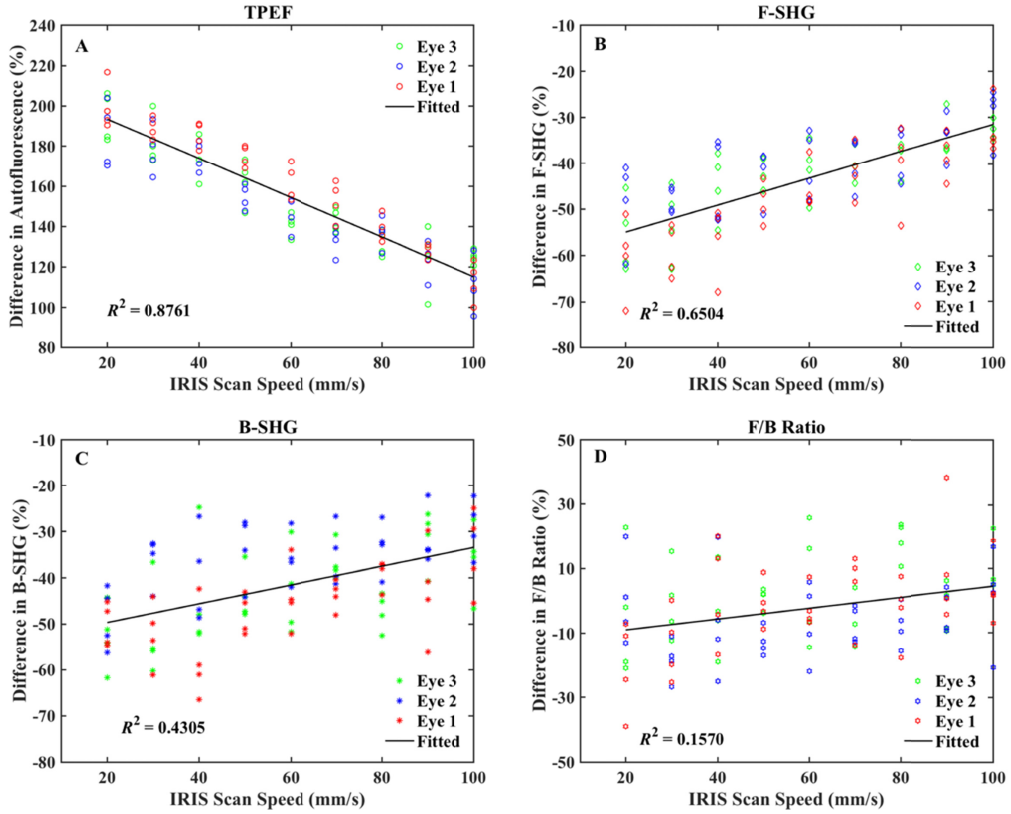

Fig. 6. Change in TPEF (a), F-SHG (b), B-SHG intensity (**c**), and F/B ratio (d) as a function of IRIS scan speed. Linear least-square fitting was performed using all the data points from three eyes, with R^2 values indicated in each graph.

Quantitative analysis showed that the local TPEF of the stroma was significantly enhanced after IRIS, and the lower the scan speed, the higher the fluorescence intensity (Fig. 6(a)). Since the change in TPEF was correlated to IRIS scan speed ($p_{\text{scan speed}} < 0.0001$, $p_{\text{eye number}} < 0.0001$, $F_{\text{scan speed}} = 734.06$, $F_{\text{eye number}} = 11.72$), it also varied as a function of induced phase change, based on the phase change profile demonstrated in part 3.1. To better understand the relationship between RI change and collagen structural alteration, we also quantified different SHG variables using co-located SHG images from the same samples (Figs. 6(b) - 6(d)). In contrast to the increase in autofluorescence, F-SHG ($p_{\text{scan speed}} < 0.0001$, $p_{\text{eye number}} < 0.0001$, $F_{\text{scan speed}} = 175.32$, $F_{\text{eye number}} = 11.38$) decreased with IRIS scan speed, and for all nine patterns investigated, the decrease in F-SHG ranged between 30% - 60%. Interestingly, the trend of decreasing B-SHG ($p_{\text{scan speed}} < 0.0001$, $p_{\text{eye number}} < 0.0001$, $F_{\text{scan speed}} = 52.35$, $F_{\text{eye number}} = 16.47$) with increasing phase change was not as clear as for F-SHG, with much lower R^2 values for B-SHG (Fig. 6(c)). As a result, the F/B ratio ($p_{\text{scan speed}} = 0.0004$, $p_{\text{eye number}} < 0.0001$, $F_{\text{scan speed}} = 13.32$, $F_{\text{eye number}} = 4.36$) did not change significantly after IRIS.

4. Discussion

The present set of experiments was designed to quantify Blue-IRIS-induced RI changes in the cornea and analyze its tissue effects using TPEF and SHG imaging. Phase changes induced by Blue-IRIS were found to decrease linearly with the laser's scan speed. Based on our previous experiments in hydrogels [4,25], we know that the magnitude of induced optical phase change is primarily determined by a combination of laser power, the geometry of written structure and scan speed. Scan speed, in particular, contributes to phase change by

Biomedical Optics EXPRESS

affecting the pulse energy deposited at each point within IRIS lines. Because of the eye's exposure limit, the entire IRIS process needs to be as fast as possible. However, sufficient power is also needed to induce localized nonlinear absorption. Therefore, with the laser power fixed, a relationship between phase change and scan speed acts as a useful calibration function for the induction of refractive structures in the cornea.

The effects of Blue-IRIS on collagen fibrillar organization were studied using both TPEF and SHG microscopy. Compared to the native corneal stroma, IRIS treated regions were characterized by a dramatic increase in TPEF. Because phase change is a monotonically decreasing function of scan speed, it can be deduced from the quantification results of fluorescence intensity that below the optical breakdown threshold, the higher the induced RI change, the stronger the autofluorescence in treated zones. For the patterns written at 100 mm/s, whose phase changes were too low to be resolved on the MZI, a ~115% increase in TPEF was still observed. Therefore, at 100 mm/s, the IRIS process may have altered protein structure in the corneal extracellular matrix in a manner sufficient to change its fluorescence but insufficient to alter the material's RI. Corneal fluorescence originates from the endogenous fluorophores physiologically present in corneal structures [29], and this enhancement was associated with possible photochemical reactions in macromolecules following laser irradiation. Vogel *et al.* and Wang *et al.* reported that free electrons can be generated via multiphoton ionization even when the femtosecond irradiation energy was below the optical breakdown threshold. This ionization field could trigger molecular reactions in the focal volume without introducing damaging thermoacoustic and shock waves [24,30]. Hovhannisyan *et al.*, reported a substantial autofluorescence increase in type I collagen from rat tail tendon and bovine Achilles' tendon under 780 nm, 120 fs laser pulse illumination. They hypothesized that the observed increase of autofluorescence was due to the formation of bi-tyrosine structures, a laser-induced photo-modification affected by both the concentration of native collagen and the amount of photoproducts present [31,32]. Tyrosine is a hydrophobic aromatic amino acid and the main chromophore of collagen molecules [33]. A spectroscopic study from Wisniewski *et al.* stated that tyrosine exhibited a higher quantum yield of fluorescence compared with other amino acids in collagen polypeptide chain [34]. Manickavasagam *et al.* studied the laser irradiated collagen degradation of acellular type I collagen gels and noticed a similar phenomenon when gels were point-irradiated using infrared femtosecond lasers [35]. Drawing from previous studies, it may be that the increased autofluorescence in IRIS regions can be attributed to the photo-degradation of collagen fibrils, and the formation of new fluorophores - perhaps tyrosine dimers - in Blue-IRIS-treated zones [36].

Besides changes in molecular composition suggested by TPEF, SHG offers another perspective on potential alterations in collagen structure at the fibrillar level. As can be seen from Fig. 5, IRIS patterns, especially those with higher phase change, can be easily distinguished from the native stroma in SHG images, with a noticeable suppression of SHG signal in IRIS-treated regions. Quantitative analysis of SHG showed that larger phase changes were associated with larger decreases of F-SHG compared to B-SHG intensity. At the macromolecular level, the elementary source of efficient second harmonic emission in collagen molecules results from the peptide bonds along the three helical chains, even though individual molecules are un-observable by SHG [37,38]. Weakening of F-SHG suggests a loss of the non-centrosymmetric collagen organization in IRIS-treated regions of the stroma, likely caused by alteration of the triple helix structure. We have done an extensive study of the changes in the collagen fibrillar organization using transmission electron microscopy (TEM). This study was done under similar conditions and supports our interpretation of the decrease in SHG [39,40]. In this study TEM, chemical hybridization and immunohistochemistry were used to show significant disruption and alteration of collagen organization in Blue-IRIS treated regions of the cornea. TEM revealed that both the pseudo-hexagonal arrangement of collagen fibrils and collagen D-banding were lost in Blue-IRIS

Biomedical Optics EXPRESS

regions. The TPEF/SHG results in the present manuscript represent an additional "signature" of these ultrastructural changes, confirming with a different approach that IRIS causes highly localized loss of fibrillar structure.

Analysis of B-SHG revealed a lack of significant change as a function of IRIS scan speed. B-SHG signals can be detected if the axial distance between adjacent sources is smaller than the coherence length of the scattering process, which is a function of the excitation and emission wavelengths [19,41,42]. It is known that corneal collagen fibrils are built from about 4 - 8 nm wide microfibrils that are stabilized by covalent intermolecular and intramolecular crosslinking [43]. With microfibrils aligned to the fibril long axis, this super-helical fibrillar structure exhibits a ~65 nm axial periodicity and each fibril acts as a scatter of incoming waves [44,45]. The lack of a statistically significant change in difference in B-SHG intensity as a function of IRIS scan speed suggests that there was no significant change in the spaces between neighboring fibrils. This, combined with the significant change in F-SHG further suggests that spatial disorder of fibrils, but not interfibrils spacing, is likely the key contributor to the observed SHG suppression.

The ratio of F-SHG to B-SHG ranged between 0.79 and 1.19 in IRIS-treated regions and did not vary significantly with IRIS scan speed, nor compared to the natural stroma. Although F/B ratio can provide information on the length scale of sources along the optical axis, different properties such as fibril thickness, ratio of different collagen components, and regularity *versus* irregularity are all possible causes for alterations of F/B ratio [17]. Therefore, at this stage, based on the F/B ratio results, we cannot determine which of these structural properties, if any, were altered after IRIS.

Depending on the deposited laser energy and tissue optical properties, laser-tissue interactions can result in either photochemical or thermal reactions. Under the breakdown threshold, chemical effects or reactions can be induced within tissues in the photochemical regime; in contrast, thermal modification features the denaturation of proteins or tissue removal after moderate temperature increase [46]. Thermal denaturation normally involves heat generation and dissipation during the interactions between tightly focused laser pulses and collagen. Thermal effects could disrupt the collagen matrix via conduction. However, under the damage threshold, this generally cannot introduce significant change in SHG signal since it does not alter the interatomic bonds in collagen molecules [35]. Additionally, an earlier study showed that during collagen thermal denaturation, SHG suppression was accompanied by a decrease in fluorescence, which was caused by the thermal decomposition of the fluorophores [47]. Since the change in IRIS-induced SHG intensity was opposite to that of autofluorescence, Blue-IRIS most likely leads to a photochemical (rather than thermal) degradation of stromal collagen fibril organization.

When analyzing how SHG intensity correlates with IRIS-induced RI change, one limitation lies in the quantification of the absolute SHG intensity of regions outside the IRIS zones. As illustrated by the F-SHG and B-SHG images in Fig. 5, collagen fibers in the anterior stroma are more randomly organized and more densely-packed than those in the posterior stroma; this inhomogeneous distribution can lead to variation of the SHG intensity at different optical planes. Therefore, instead of measuring the average pixel intensity of the entire image, similar size of ROIs at the same axial depth were quantified and defined as the SHG intensity from regions outside the IRIS zones. However, partial corneal tissue was lost in some samples during the cryostat sectioning, which introduced a larger deviation of the SHG intensity change than that of the fluorescence intensity. Nevertheless, compared with the qualitative approach generally used in multiphoton microscopy imaging studies, the present study illustrates that it is possible to use quantifiable SHG parameters to discriminate different refractive phase structures, and that the dual-modal imaging method hereby described can provide useful, complementary insights into structural changes of the corneal collagen matrix.

Biomedical Optics EXPRESS

5. Conclusion

The present set of experiments allowed us to build a phase change profile for Blue-IRIS as a function of scan speed in the living cornea, using it to calibrate changes in SHG images for the first time. Approximately 0.51 waves of phase change could be obtained from IRIS when writing at 20 mm/s with 82 mW laser power, corresponding to a RI change of + 0.011. The effects of Blue-IRIS on corneal collagen organization were studied using simultaneous TPEF and SHG microscopy. By quantifying the intensity difference between IRIS-treated and untreated regions of the cornea, a significant increase in autofluorescence and decrease of SHG signals were observed in proportion to the increased phase change. This work provides compelling evidence that considering F-SHG as well as B-SHG in a quantitative manner can give useful insights into corneal collagen structure. We believe this particular combination of TPEF and SHG signatures indicates that Blue-IRIS modified the organization of collagen triple helices at a molecular level, and that this caused degradation of collagen fibril arrangement. Ongoing research is seeking to ascertain more specifically what features of the collagen microstructure, *e.g.* fibril density, diameter, direction, and molecular composition, are modified by Blue-IRIS. These findings provide valuable insights into potential photophysical mechanisms by which Blue-IRIS induces a RI change in the cornea.

Funding

NYSTAR Center for Emerging and Innovative Sciences (CEIS); Clerio Vision, Inc.; National Institutes of Health (NIH) (P30 EY001319); NIH (EY015836); the Research to Prevent Blindness Foundation

Acknowledgments

The authors would like to thank Margaret DeMagistris for technical support in tissue preparation, Tracy Bubel for tissue processing, corneal sectioning and Dr. Paul D. Funkenbusch for support in statistics analysis.

Disclosures

Wayne H. Knox: Clerio Vision, Inc. (F, I, C, P, R), Krystel R. Huxlin: Clerio Vision, Inc. (F, I, P).

References

1. L. Ding, R. Blackwell, J. F. Kunzler, and W. H. Knox, "Large refractive index change in silicone-based and non-silicone-based hydrogel polymers induced by femtosecond laser micro-machining," Opt. Express **14**(24), 11901–11909 (2006).
2. L. Ding, L. G. Cancado, L. Novotny, W. H. Knox, N. Anderson, D. Jani, J. Linhardt, R. I. Blackwell, and J. E. Kiinzler, "Micro-Raman spectroscopy of refractive index microstructures in silicone-based hydrogel polymers created by high-repetition-rate femtosecond laser micromachining," J. Opt. Soc. Am. B **26**(4), 595–602 (2009).
3. L. J. Nagy, L. Ding, L. Xu, W. H. Knox, and K. R. Huxlin, "Potentiation of Femtosecond Laser Intratissue Refractive Index Shaping (IRIS) in the Living Cornea with Sodium Fluorescein," Invest. Ophthalmol. Vis. Sci. **51**(2), 850–856 (2010).
4. L. Xu, W. H. Knox, M. DeMagistris, N. Wang, and K. R. Huxlin, "Noninvasive Intratissue Refractive Index Shaping (IRIS) of the Cornea with Blue Femtosecond Laser Light," Invest. Ophthalmol. Vis. Sci. **52**(11), 8148–8155 (2011).
5. D. E. Savage, D. R. Brooks, M. DeMagistris, L. Xu, S. MacRae, J. D. Ellis, W. H. Knox, and K. R. Huxlin, "First demonstration of Ocular Refractive Change Using Blue-IRIS in Live Cats," Invest. Ophthalmol. Vis. Sci. **55**(7), 4603–4612 (2014).
6. K. T. Wozniak, N. Elkins, D. R. Brooks, D. E. Savage, S. MacRae, J. D. Ellis, W. H. Knox, and K. R. Huxlin, "Contrasting cellular damage after Blue-IRIS and Femto-LASIK in cat cornea," Exp. Eye Res. **165**, 20–28 (2017).
7. G. A. Gandara-Montano, V. Stoy, M. Dudic, V. Petrak, K. Haskovcova, and W. H. Knox, "Large optical phase shifts in hydrogels written with femtosecond laser pulses: elucidating the role of localized water concentration changes," Opt. Mater. Express **7**(9), 3162–3180 (2017).
8. G. Wollensak and E. Iomdina, "Long-term biomechanical properties of rabbit sclera after collagen crosslinking using riboflavin and ultraviolet A (UVA)," Acta Ophthalmol. **87**(2), 193–198 (2009).

Biomedical Optics EXPRESS

9. J. L. Ojeda, J. A. Ventosa, and S. Piedra, "The three-dimensional microanatomy of the rabbit and human cornea. A chemical and mechanical microdissection-SEM approach," J. Anat. **199**(5), 567–576 (2001).
10. F. Aptel, N. Olivier, A. Deniset-Besseau, J. M. Legeais, K. Plamann, M. C. Schanne-Klein, and E. Beaurepaire, "Multimodal Nonlinear Imaging of the Human Cornea," Invest. Ophthalmol. Vis. Sci. **51**(5), 2459–2465 (2010).
11. J. M. Dela Cruz, J. D. McMullen, R. M. Williams, and W. R. Zipfel, "Feasibility of using multiphoton excited tissue autofluorescence for in vivo human histopathology," Biomed. Opt. Express **1**(5), 1320–1330 (2010).
12. L. Cui, K. R. Huxlin, L. Xu, S. MacRae, and W. H. Knox, "High-resolution, noninvasive, two-photon fluorescence measurement of molecular concentrations in corneal tissue," Invest. Ophthalmol. Vis. Sci. **52**(5), 2556–2564 (2011).
13. W. R. Zipfel, R. M. Williams, and W. W. Webb, "Nonlinear magic: multiphoton microscopy in the biosciences," Nat. Biotechnol. **21**(11), 1369–1377 (2003).
14. X. Han and E. Brown, "Measurement of the ratio of forward-propagating to back-propagating second harmonic signal using a single objective," Opt. Express **18**(10), 10538–10550 (2010).
15. X. Chen, O. Nadiarynkh, S. Plotnikov, and P. J. Campagnola, "Second harmonic generation microscopy for quantitative analysis of collagen fibrillar structure," Nat. Protoc. **7**(4), 654–669 (2012).
16. R. M. Williams, W. R. Zipfel, and W. W. Webb, "Interpreting second-harmonic generation images of collagen I fibrils," Biophys. J. **88**(2), 1377–1386 (2005).
17. R. Lacomb, O. Nadiarnykh, S. S. Townsend, and P. J. Campagnola, "Phase matching considerations in second harmonic generation from tissues: Effects on emission directionality, conversion efficiency and observed morphology," Opt. Commun. **281**(7), 1823–1832 (2008).
18. W. R. Zipfel, R. M. Williams, R. Christie, A. Y. Nikitin, B. T. Hyman, and W. W. Webb, "Live tissue intrinsic emission microscopy using multiphoton-excited native fluorescence and second harmonic generation," Proc. Natl. Acad. Sci. U.S.A. **100**(12), 7075–7080 (2003).
19. T. A. Theodossiou, C. Thrasivoulou, C. Ekwobi, and D. L. Becker, "Second harmonic generation confocal microscopy of collagen type I from rat tendon cryosections," Biophys. J. **91**(12), 4665–4677 (2006).
20. X. Han, R. M. Burke, M. L. Zettel, P. Tang, and E. B. Brown, "Second harmonic properties of tumor collagen: determining the structural relationship between reactive stroma and healthy stroma," Opt. Express **16**(3), 1846–1859 (2008).
21. Y. Suzaki and A. Tachibana, "Measurement of the Mu-M Sized Radius of Gaussian Laser Beam Using the Scanning Knife-Edge," Appl. Opt. **14**(12), 2809–2810 (1975).
22. M. S. Scholl, "Measured Spatial Properties of the cw Nd:YAG Laser Beam," Appl. Opt. **19**(21), 3655–3659 (1980).
23. R. L. Lindstrom, H. E. Kaufman, D. L. Skelnik, R. A. Laing, J. H. Lass, D. C. Musch, M. D. Trousdale, W. J. Reinhart, T. E. Burris, A. Sugar, R. M. Davis, K. Hirokawa, T. Smith, and J. F. Gordon, "Optisol Corneal Storage Medium," Am. J. Ophthalmol. **114**(3), 345–356 (1992).
24. A. Vogel, J. Noack, G. Huttman, and G. Paltauf, "Mechanisms of femtosecond laser nanosurgery of cells and tissues," Appl. Phys. B **81**(8), 1015–1047 (2005).
25. G. A. Gandara-Montano, A. Ivansky, D. E. Savage, J. D. Ellis, and W. H. Knox, "Femtosecond laser writing of freeform gradient index microlenses in hydrogel-based contact lenses," Opt. Mater. Express **5**(10), 2257–2271 (2015).
26. M. Takeda, H. Ina, and S. Kobayashi, "Fourier-Transform Method of Fringe-Pattern Analysis for Computer-Based Topography and Interferometry," J. Opt. Soc. Am. **72**(1), 156–160 (1982).
27. R. M. Goldstein, H. A. Zebker, and C. L. Werner, "Satellite Radar Interferometry - Two-Dimensional Phase Unwrapping," Radio Sci. **23**(4), 713–720 (1988).
28. N. Morishige, W. M. Petroll, T. Nishida, M. C. Kenney, and J. V. Jester, "Noninvasive corneal stromal collagen imaging using two-photon-generated second-harmonic signals," J. Cataract Refract. Surg. **32**(11), 1784–1791 (2006).
29. A. M. Calvo-Maroto, R. J. Perez-Cambrodi, S. Garcia-Lazaro, T. Ferrer-Blasco, and A. Cerviño, "Ocular autofluorescence in diabetes mellitus. A review," J. Diabetes **8**(5), 619–628 (2016).
30. C. Wang, M. Fomovsky, G. X. Miao, M. Zyablitskaya, and S. Vukelic, "Femtosecond laser crosslinking of the cornea for non-invasive vision correction," Nat. Photonics **12**(7), 416–422 (2018).
31. V. Hovhannisyan, W. Lo, C. Hu, S. J. Chen, and C. Y. Dong, "Dynamics of femtosecond laser photo-modification of collagen fibers," Opt. Express **16**(11), 7958–7968 (2008).
32. V. Hovhannisyan, A. Ghazaryan, Y. F. Chen, S. J. Chen, and C. Y. Dong, "Photophysical mechanisms of collagen modification by 80 MHz femtosecond laser," Opt. Express **18**(23), 24037–24047 (2010).
33. M. J. Davies and R. J. W. Truscott, "Photo-oxidation of proteins and its role in cataractogenesis," J. Photochem. Photobiol. B **63**(1-3), 114–125 (2001).
34. M. Wisniewski, A. Sionkowska, H. Kaczmarek, S. Lazare, V. Tokarev, and C. Belin, "Spectroscopic study of a KrF excimer laser treated surface of the thin collagen films," J Photoch Photobio A **188**(2-3), 192–199 (2007).
35. A. Manickavasagam, L. M. Hirvonen, L. N. Melita, E. Z. Chong, R. J. Cook, L. Bozec, and F. Festy, "Multimodal optical characterisation of collagen photodegradation by femtosecond infrared laser ablation," Analyst (Lond.) **139**(23), 6135–6143 (2014).
36. M. Oujja, E. Rebollar, C. Abrusci, A. Del Amo, F. Catalina, and M. Castillejo, "UV, visible and IR laser interaction with gelatine," J. Phys. Conf. Ser. **59**, 571–574 (2007).

Biomedical Optics EXPRESS

37. A. E. Tuer, S. Krouglov, N. Prent, R. Cisek, D. Sandkuijl, K. Yasufuku, B. C. Wilson, and V. Barzda, "Nonlinear Optical Properties of Type I Collagen Fibers Studied by Polarization Dependent Second Harmonic Generation Microscopy," J. Phys. Chem. B **115**(44), 12759–12769 (2011).
38. S. V. Plotnikov, A. C. Millard, P. J. Campagnola, and W. A. Mohler, "Characterization of the myosin-based source for second-harmonic generation from muscle sarcomeres," Biophys. J. **90**(2), 693–703 (2006).
39. D. E. Savage, "A non-ablative technique for femtosecond laser-based refractive correction: development, efficacy, and tissue effects," (University of Rochester, Rochester, N.Y., 2018).
40. D. E. Savage, University of Rochester, Rochester, N.Y. 14627, and D. R. Brooks, Y. Li, M. Yu, J. A. Weiss, W. H. Knox and K. R. Huxlin are preparing a manuscript to be called "Blue-IRIS alters corneal refractive index by changing collagen fibrillar organization."
41. G. Latour, I. Gusachenko, L. Kowalczuk, I. Lamarre, and M. C. Schanne-Klein, "In vivo structural imaging of the cornea by polarization-resolved second harmonic microscopy," Biomed. Opt. Express **3**(1), 1–15 (2012).
42. B. M. Kim, J. Eichler, and L. B. Da Silva, "Frequency doubling of ultrashort laser pulses in biological tissues," Appl. Opt. **38**(34), 7145–7150 (1999).
43. K. M. Meek and C. Knupp, "Corneal structure and transparency," Prog. Retin. Eye Res. **49**, 1–16 (2015).
44. K. M. Meek, G. F. Elliott, Z. Sayers, S. B. Whitburn, and M. H. J. Koch, "Interpretation of the Meridional X-Ray Diffraction Pattern from Collagen Fibrils in Corneal Stroma," J. Mol. Biol. **149**(3), 477–488 (1981).
45. S. Yamamoto, H. Hashizume, J. Hitomi, M. Shigeno, S. Sawaguchi, H. Abe, and T. Ushiki, "The subfibrillar arrangement of corneal and scleral collagen fibrils as revealed by scanning electron and atomic force microscopy," Arch. Histol. Cytol. **63**(2), 127–135 (2000).
46. Y. Sun, W. L. Chen, S. J. Lin, S. H. Jee, Y. F. Chen, L. C. Lin, P. T. C. So, and C. Y. Dong, "Investigating mechanisms of collagen thermal denaturation by high resolution second-harmonic generation imaging," Biophys. J. **91**(7), 2620–2625 (2006).
47. V. Hovhannisyan, W. Lo, C. Hu, S.-J. Chen, and C. Y. Dong, "Non-ablative processing of biofibers by femtosecond IR laser," in *European Conferences on Biomedical Optics*, (SPIE, 2009), 7.